Nuclear Engineering and Technology 51 (2019) 1261–1271

Contents lists available at ScienceDirect

Nuclear Engineering and Technology

journal homepage: www.elsevier.com/locate/net

Original Article

Droplet size prediction model based on the upper limit log-normal distribution function in venturi scrubber

Sang Won Lee [a], Hee Cheon No [b, *]

[a] Korea Hydro and Nuclear Power - Central Research Institute, 70 Gil, Yuseong-daero 1312, Yuseong-gu, Daejeon, 305-343, Republic of Korea
[b] Department of Nuclear and Quantum Engineering, Korea Advanced Institute of Science and Technology, Yuseong-gu, Daejeon, 305-701, Republic of Korea

ARTICLE INFO

Article history:
Received 24 January 2019
Received in revised form
11 March 2019
Accepted 18 March 2019
Available online 19 March 2019

Keywords:
Droplet size
ULLN
Breakup model
Critical Weber number

ABSTRACT

Droplet size and distribution are important parameters determining venturi scrubber performance. In this paper, we proposed physical models for a maximum stable droplet size prediction and upper limit log-normal (ULLN) distribution parameters. For the proposed maximum stable droplet size prediction model, a Eulerian-Lagrangian framework and a Reitz-Diwakar breakup model are solved simultaneously using CFD calculations to reflect the effect of multistage breakup and droplet acceleration. Then, two ULLN distribution parameters are suggested through best fitting the previously published experimental data. Results show that the proposed approach provides better predictions of maximum stable droplet diameter and Sauter mean diameter compared to existing simple empirical correlations including Boll, Nukiyama and Tanasawa. For more practical purpose, we developed the simple, one dimensional (1-D) calculation of Sauter mean diameter.

1. Introduction

The venturi scrubber is used to collect contaminated, fine particle laden material from a gas flow before it is released into the environment. The main advantages of venturi scrubber are its high filtering efficiency and low installation and maintenance costs. Accordingly, it has been widely used in various engineering fields that require the efficient filtering of fine particles.

The venturi scrubber consists of three components: a converging, throat, and diffuser section. The particle-laden gas flows into the convergent section and is accelerated in the throat. Generally, a liquid is introduced into the throat in the form of jets perpendicular to the gas flow, injected by an external pump through small orifices located in the throat side wall. These liquid jets interact with the high-velocity gas in the throat, causing breakup and atomization and generating fine droplets along the throat and diffuser. The main filtering mechanism of a venturi scrubber is inertial impaction, in which fine particles in the gas stream adhere to the surface of the atomized droplets, collecting the contaminated particles. In the diffuser section, the gas velocity decelerates for pressure recovery to minimize pumping cost [1]. Recently, venturi scrubber design has been actively considered in the nuclear field to minimize the release of aerosol-type radioactive material into the environment following a severe accident, such as the Fukushima accident [2]. The main difference between the typical application of a venturi scrubber and a nuclear industry application is that the scrubber be operated without electricity under the accident condition. To provide this capability, it has been proposed that the venturi scrubber be submerged inside the pool where water can passively flow into the scrubber throat under the effects of gravity head, compared the forced jet feeding used in a conventional venturi scrubber [3,4] as shown in Fig. 1.

The performance of the venturi scrubber has been extensively investigated for several decades to determine the optimal filtering efficiency for the lowest operating cost. Several major parameters influencing the collection efficiency and pressure drop have been identified, including droplet size and distribution inside the venturi scrubber. Therefore, accurate prediction of the size and distribution of droplets is important in enhancing the performance of a venturi scrubber.

Many factors affect the droplet size inside a venturi scrubber depending on the operating conditions, including gas velocity, the ratio of liquid flow to gas flow (L/G), and orifice geometry. These conditions affect physical phenomena such as primary and secondary atomization, coalescence of droplets, the sizes of droplets, and droplets deposition on the interior walls of the scrubber [1]. Therefore, the purpose of this study is to propose and evaluate an improved method for determining the droplet size and its

* Corresponding author.
E-mail address: hcno@kaist.ac.kr (H.C. No).

https://doi.org/10.1016/j.net.2019.03.014

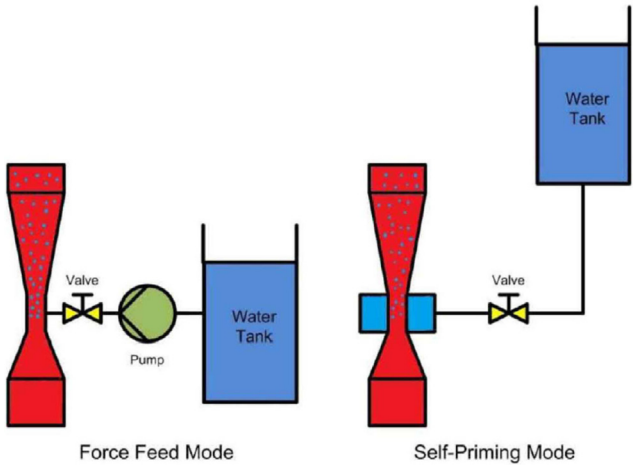

Fig. 1. Schematics of forced feed and self-priming mode of venturi scrubber [2,3].

distribution in a venturi scrubber.

2. Literature review

Various studies have been performed to determine the representative size of droplets in a venturi scrubber. Most of these previous studies have used the sauter mean diameter (D_{32}) as a representative droplet size [5]. A number of empirical correlations have been proposed to adjust the D_{32} obtained using experimental measurements [6]. Widely used empirical correlations were provided by Nukiyama and Tanasawa [7], and by Boll et al. [8]. The Nukiyama and Tanasawa (NT) correlation was developed based on data collected from annular flow in plain tubes with an experimental range of gas velocity from 73 to 230 m/s and an L/G of 0.8–1.0 liter/m^3, and can be described as follows:

$$D_{32} = \frac{0.585}{u_g}\sqrt{\frac{\sigma}{\rho_l}} + 1.683 \times 10^{-3}\left(\frac{\mu_l}{\sqrt{\sigma\rho_l}}\right)^{0.45}(L/G)^{1.5} \quad (1)$$

Boll's correlation was derived using commercial-scale venturi scrubber geometry with an experimental range of gas throat velocity of 30–90 m/s and an L/G of 0.6–2.5 liter/m^3 as follows:

$$D_{32} = \frac{4.22 \times 10^{-2} + 5.77 \times 10^{-3}(L/G)^{1.922}}{u_g^{1.602}} \quad (2)$$

Both correlations are typically written as two-term equations in which the first term reflects the decrease in droplet size as the gas velocity increases due to the breakup mechanism and the second term reflects the effect of L/G due to coalescence [9].

Another important physical parameter affecting droplet size is the maximum stable droplet diameter, D_{max}. The representative non-dimensional parameter related to D_{max} is the critical Weber number. The initial Weber number can be expressed as a balance between disruptive hydro-dynamic forces and the stabilizing surface tension force at the droplet injection location as follows:

$$We = \frac{\rho_g U_{r,0}^2 D_0}{\sigma} \quad (3)$$

where $U_{r,o}$ is the initial relative velocity and D_o is the initial droplet diameter.

The critical Weber number We_{crit} has been experimentally studied and determined to be approximately 12 [10]. Based on the definition of the initial Weber number, the maximum stable droplet diameter can thus be expressed as:

$$D_{max} = We_{crit}\frac{\sigma}{\rho_g U_{r,0}^2} \quad (4)$$

Pilch and Erdman [11] argued that the value of D_{max} calculated using Eq. (4) is significantly underestimated compared to experimental data because it assumes instantaneous, complete breakup of the droplet at its initial position. Indeed, experimental evidence has shown that breakup actually occurs over a specific period of time called the total breakup time. The breakup of a droplet with a large Weber number occurs through a multistage process in which the droplet undergoes continued breakup until its Weber number decreases below the critical Weber number. Accordingly, Pilch and Erdman [11] suggested an expression for D_{max} that reflects the effects of droplet acceleration and the decrease in relative velocity between the droplet and gas flow during breakup considering the local Weber number as follows:

$$D_{max} = We_{crit}\frac{\sigma}{\rho_g U_{r,0}^2}\left(1 - \frac{U_d}{U_{r,0}}\right)^{-2} = We_{crit}\frac{\sigma}{\rho_g (U_{r,0} - U_d)^2} \quad (5)$$

where U_d is the velocity of the droplet once all breakup processes have terminated. To obtain U_d, Pilch and Erdman [11] suggested a correlation between total breakup time and droplet acceleration based on a modified momentum equation. Results show that this approach provides a better prediction capability of droplet size for large Weber numbers.

Another important research area is the droplet size distribution. Various experimental results show that the droplet size has its own distribution. Information on droplet size distribution is useful in fundamental analyses of the transport of mass or heat in a dispersed flow [12]. Another advantage of knowing the droplet size distribution is that various information on droplet size, including the mass mean diameter and volume mean diameter, can be obtained using mathematical relationships. The use of a D_{32} instead of droplet size distribution inside the venturi scrubber has been reviewed by Bayvel [13], who concluded that the calculated overall collection efficiency would be different if the size distribution was used instead of the D_{32}.

Several theoretical droplet distribution functions have been accordingly proposed to fit experimentally obtained droplet distribution data. Widely used distributions are the Rosin-Rammler (RR) distribution and the upper limit log-normal (ULLN) distribution [14].

The RR distribution is a single-peaked distribution function utilized when analyzing sprays [15]. In its cumulative form, this volume distribution function is expressed as:

$$F_3(d) = 1 - \exp\left[\left(d/\overline{d}\right)^q\right] \quad (6)$$

Where $\overline{d}$ is the diameter that 63.2% of the total mass is in smaller than, and q is the distribution parameter. The higher the value of q, the more uniform the droplet size distribution. The D_{32} can be obtained using RR distribution parameter and mathematical gamma function:

$$D_{32} = \overline{d}\Big/\Gamma\left(1 - 1/q\right) \quad (7)$$

Mugele and Evans [12] reviewed several size distribution functions for dispersed flow and their application to experimental data, proposing a modification of the existing log-normal probability distribution function, called the ULLN distribution, for the distribution of droplet size in sprays. The ULLN distribution for atomizing jets has been applied by several investigators to their experimental

data in annular dispersed flow [14]. This distribution is given in the following equation in a probabilistic distribution form:

$$f_3(d) = \frac{\delta D_{max}}{\sqrt{\pi} d(D_{max}-d)} exp\left\{ -\delta^2 \left[\ln\left(\frac{ad}{D_{max}-d}\right)\right]^2 \right\} \quad (8)$$

where, $a = \frac{d_{max}}{d_{v50}} - 1$, $\delta = \frac{0.394}{log\left\{\frac{d_{v90}/(d_{max}-d_{v90})}{d_{v50}/(d_{max}-d_{v50})}\right\}}$, d_{v50} is the volume median diameter, and δ is the distribution parameter.

The expression in Eq. (8) introduced three distribution parameters, including a new and physically significant parameter D_{max}. All the distribution functions except for the ULLN distribution have an infinite D_{max}, but it remains physically reasonable to include the D_{max} to maintain theoretical completeness.

Mugele and Evans [12] found that δ and a would only be weakly dependent on the flow variables of annular flows by comparing the experimental results. The sensitivities of δ and a are shown in Fig. 2. In this figure, x axis is the normalized droplet diameter representing the ratio of droplet diameter to D_{max} and y axis is the probabilistic distribution. Several researchers have proposed ULLN distribution parameters based on existing experimental data, as summarized in Table 1.

The relationship between D_{max} and D_{32} can be easily derived mathematically as:

$$\frac{D_{32}}{D_{max}} = \frac{1}{\left(1 + ae^{1/4\delta^2}\right)} \quad (9)$$

Table 1
Suggested ULLN distribution parameters.

Study	a	δ	Experimental data used
Tatterson [16]	1.9	0.72	Wicks [17], Cousins [18], Tatterson [16]
Kocanustafaogullari [20]	1.93	0.75	Wicks [17], Cousins [18], Lopes [19]
Hay [21]	2.6	0.84	Hay [21]

3. Droplet size prediction model for CFD with ULLN distribution parameters

We developed a calculation methodology for D_{max} using a computational fluid dynamic (CFD) approach with Lagrangian particle tracking coupled with a particle breakup model. Also, we proposed ULLN distribution parameters using the best fit of experimentally determined D_{32} values.

3.1. CFD model

Computational fluid dynamic methods have been widely used to predict complex thermo-hydraulic behavior and to optimize component design. To calculate venturi scrubber performance, two components, the gas flow and the droplet, should be analyzed. For the gas flow, the Eulerian approach is used as a continuous phase. The methods used to calculate droplet behavior are divided into two types. The first type is the Eulerian approach, which has been used in some researches [22] as it can predict the average properties of droplets such as velocity, mass, temperature, and volume fraction using partial differential equations. The advantage of this method is its relatively simple modeling and fast running time with reasonable prediction results. However, this approach does not predict detailed particle behaviors, such as the breakup of the droplet, interfacial area, and filtering efficiency. The second type of droplet behavior calculation is the Lagrangian particle tracking method, which tracks all the droplets injected into the domain as moving mass points using ordinary differential equations. No volume is occupied by the droplets in the continuous field; they instead work as momentum sinks [23]. The calculation of the behavior of all the droplets is nearly impossible and even unnecessary. So the parcel concept of using one representative particle for each tracking path has been introduced. Using this concept, for a certain particle tracking path, the mass flow rate is conserved while both the representative droplet diameter and particle number rate can change. The particle momentum sources consist of several terms including drag force, buoyancy force, and virtual mass force. In this calculation, only drag force is considered because it is dominant in the breakup using the following equations [24]:

$$U_d = \frac{dx_i}{dt} \quad (10)$$

$$\dot{n}_d = \frac{\dot{m}_d}{m_d} \quad (11)$$

$$\frac{dS}{dt} = -F_D = -\frac{1}{2} C_D \rho_d A_d |U_g - U_d| (U_g - U_d) \dot{n}_d \quad (12)$$

where, for a single droplet mass, $m_d = \frac{4}{3}\pi r^3 \rho_d$, and $\dot{m}_d$ is the droplet mass flow-rate for an individual particle tracking path. The momentum source term in Eq. (12) is coupled to the momentum equation for the Eulerian gas flow field and a fully coupled calculation scheme is used for the convergence criteria. In this paper, a combined Eulerian-Lagrangian approach is used in which the gas flow field is solved using the Eulerian framework and the droplet behaviors are solved based on the

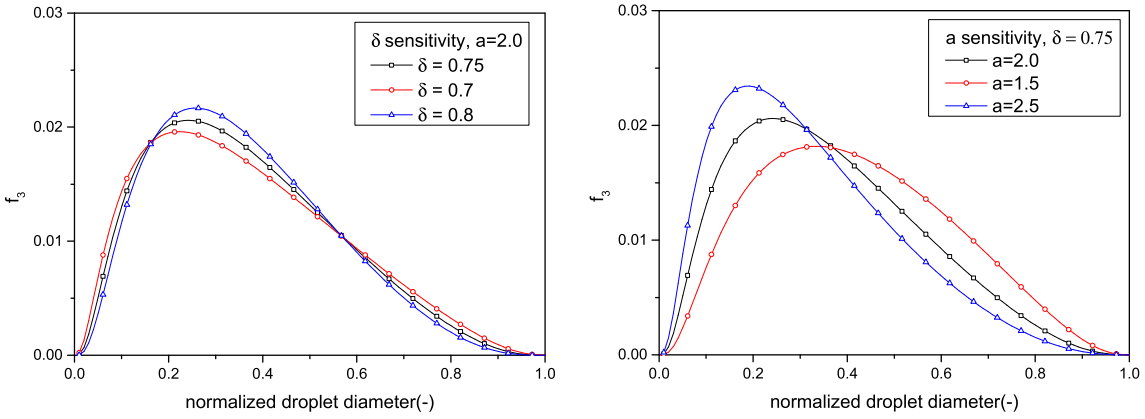

Fig. 2. Sensitivity of ULLN distribution parameters.

Table 2
Reitz-Diwakar breakup model.

	Bag Breakup	Stripping Breakup
Criterion for breakup mechanism	$We > We_{crit} = 12$	$We/\sqrt{Re_d} > 0.5$
Life time of unstable droplet	$\tau_b = \pi\sqrt{\frac{\rho_d\left(D_d/2\right)^3}{2\sigma_d}}$	$\tau_b = 20\frac{D_d/2}{V_r}\sqrt{\frac{\rho_d}{\rho_g}}$
Stable droplet diameter	$D_{d,\,stable} = We_{crit}\frac{\sigma}{\rho_g U_r^2}\,(We_{crit} = 12,\ default)$	$D_{d,stable} = \frac{\sigma^2}{\rho_g U_r^3 \mu_g}\,(We/\sqrt{Re_d} = 0.5)$

Table 3
Problem setup for CFD calculations.

Parameter	Value
Pressure/temperature	0.1 MPa, 25 °C
Geometry	Pipe diameter: 0.095 m Pipe length: 3 m Injection location: 0.5 m
Working fluid	Water/air
Fluid modeling method	Gas: Eulerian Droplet: Lagrangian particle tracking
Initial droplet diameter	2 mm (orifice diameter)
Total Lagrangian particle path	10,000
Primary breakup model	Blob
Secondary breakup model	Reitz-Diwakar
Initial droplet rate	10 per particle path
Turbulent modeling	SST
No. of elements in mesh	970,000

Lagrangian framework.

The droplet breakup model is divided into primary and secondary breakup stages. Primary breakup represents the breakup of the liquid jet at the nozzle exit that initially generates droplets, after which secondary breakup occurs downstream. If the orifice geometry is pressure swirl atomizer or nozzle cavitation is expected, the initial droplet size might be different to the orifice size. In this calculation we assume the simple orifice geometry.

So, the blob model, one of the simplest models, which assume the nozzle diameter as the initial droplet diameter, is used to describe primary breakup.

The secondary breakup model considers the deformation of the initial spherical shape of the droplet and its atomization due to the turbulence of the gas and external aerodynamic forces acting on the droplet. The main objective of the secondary breakup model is to determine the stable droplet size. There are several models available, including those proposed by Reitz and Diwakar [25] and Schmehl et al. [26], as well as the Cascade atomization and breakup model [27].

Stability criteria for Reitz-Diwakar model is exactly same as a critical Weber number definition. This means that the Reitz-Diwakar model is physically reasonable for predicting D_{max} rather than D_{32}. Therefore, we use Reitz-Diwakar model to calculate D_{max}. This model assumes the breakup to be a multistage process in which the droplets undergo further breakup until their local Weber number decreases below the critical Weber number as indicated by Pilch and Erdman [11]:

$$\frac{dD_d}{dt} = -\frac{D_d - D_{d,stable}}{\tau_b} \tag{13}$$

The RD model was developed based on the experiments of Reinecke and Waldman [28] on the breakup of isolated drops and the correlations given by Nicholls [29]. Breakup mechanisms are classified as either stripping breakup or bag breakup based on the local Weber number. In stripping breakup, liquid is sheared from the periphery of the deforming drop surface in a high Weber number. In bag breakup, a thin hollow bag is blown downstream

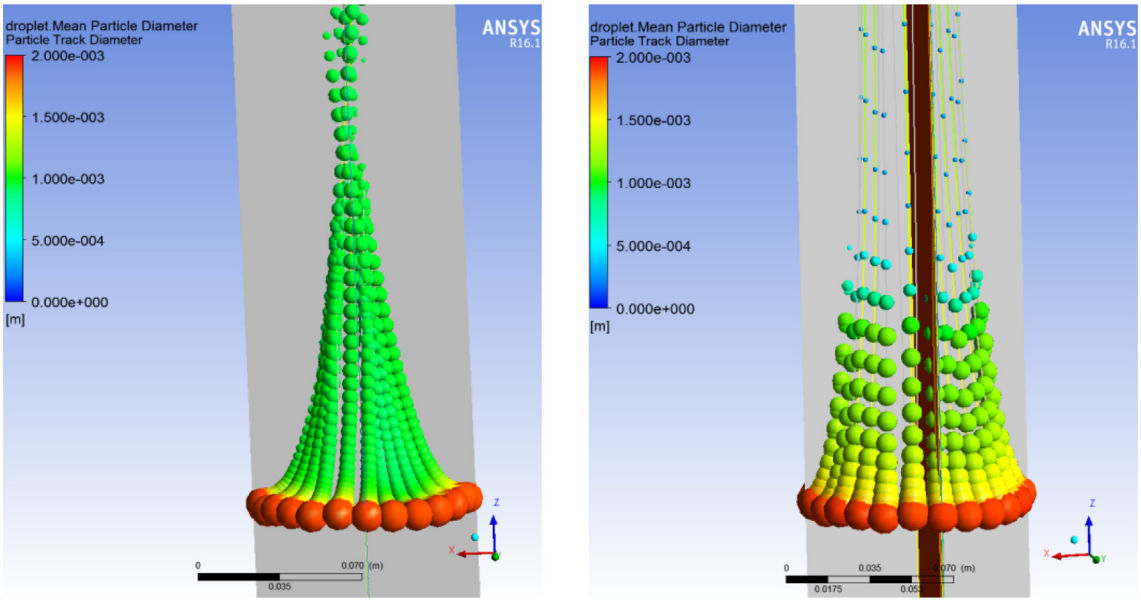

(a) Vg = 30 m/s (b) Vg = 75 m/s

Fig. 3. Droplet breakup behavior over the particle tracking path.

while it is attached to a toroidal rim. The bag eventually bursts, forming a large number of small droplets. It occurs at relatively a low Weber number [11].

In the CFD calculation, each cell has information on the gas velocity, droplet velocity, and droplet size. So, the local Weber number can be easily calculated.

The criterion for breakup mechanism selection is checked for each drop parcel at each time step, and the droplet diameter is calculated against each mechanism using Eq. (13) based on the calculation of the lifetime of an unstable droplet and the stable droplet diameter as summarized in Table 2.

As shown in Table 2, according to the definition of stable droplet diameter under bag breakup, the final droplet size is determined when the local Weber number converges to the critical Weber number. This means that the RD model is physically reasonable for predicting D_{max} rather than D_{32}. Therefore, in the CFD calculation of this study, the calculated droplet diameter is defined as D_{max}.

In this study, particles are assumed to be spherical. The drag coefficient of a spherical particle has been extensively studied and is proposed to be a function of the droplet Reynolds number. The widely used Shiller-Naumann correlation is applied in this study as follows:

$$C_D = \frac{24}{Re_d}\left(1 + 0.15Re_d^{0.687}\right) \tag{14}$$

where the droplet Reynolds number $Re_d = \frac{\rho_g D_d |U_g - U_d|}{\mu_g}$

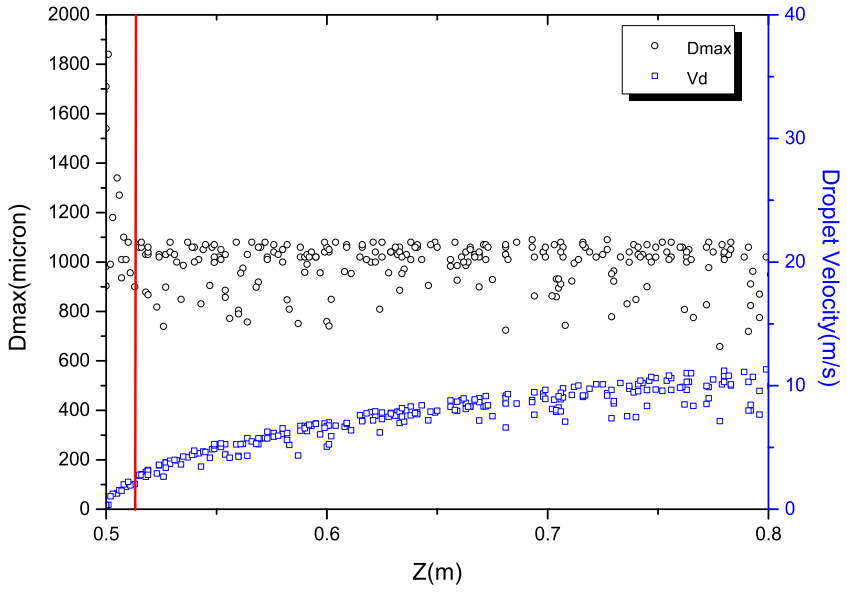

(a) *Vg* = 30 m/s

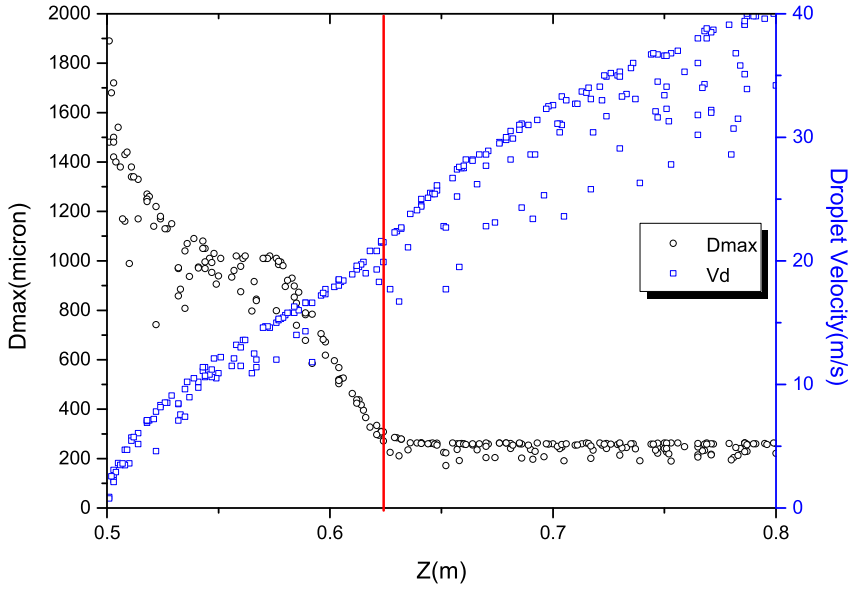

(b) *Vg* = 75 m/s

Fig. 4. Droplet velocity and diameter in the axial direction.

There are various kinds of different geometry used for the venturi scrubber. However, droplet breakup is mainly influenced by the relative velocity between the gas and the droplet. The objective of this CFD calculation is to determine the D_{max} during multistage breakup and to reflect the effect of droplet acceleration considering breakup time and local Weber number. For this general application, a simple straight pipe is modeled to predict D_{max} for isolated droplet breakup. Gas velocity at the throat inlet is used as an initial condition to calculate the local gas velocity and local droplet velocity inside venturi scrubber considering droplet breakup. Then relative velocity obtained are used to determine the D_{max}.

A three-dimensional straight pipe was generated using the ANSYS CFX 16 software package. The hybrid meshes, consisting of tetrahedrons and prisms, contained 970,000 elements. The convergence criteria for simulations were 10^{-5} RMS for the residuals. For turbulence modeling, the well-known SST was used. The turbulence increases due to the relative velocity between gas and droplet due to interfacial drag and breakup. In respect to the turbulence in particle tracking in CFX, the instantaneous fluid velocity is decomposed into mean velocity and fluctuating component. The particle has no volume occupied and just work as a momentum source. Particle follows separate trajectories due to the random nature of the instantaneous fluid velocity. It is the fluctuating component of the fluid velocity that causes the dispersion of particles in a turbulent flow [24]. For the boundary condition at the inlet, the mass flow rate of the gas was applied. The droplet was injected as a particle transport fluid with a mass flow rate boundary condition and a total of 10,000 parcels. At the outlet, the pressure boundary condition was used. The detailed problem setup is summarized in Table 3.

3.2. Calculation results by CFD

Fig. 3 shows the representative Lagrangian particle tracking behaviors of a droplet. Two gas velocity cases are compared: a low gas velocity *Vg* of 30 m/s and high gas velocity *Vg* of 75 m/s. The breakup of each droplet diameter along the particle tracking paths is shown over a time span of 0.001 s. The first circle that leaves the orifice is primary breakup, and the rest of them are all secondary breakup. In the case shown in Fig. 3(a), the droplet diameter reaches its stable condition almost instantaneously. The case shown in Fig. 3(b), in contrast, shows continuous breakup occurring further downstream of the injection location until reaching stable condition.

Fig. 4 shows the droplet velocity and diameter along the z direction. In the case shown in Fig. 4(a), the droplet reaches its stable condition within 0.02 m beyond the injection location because the local Weber number reaches the critical Weber number. At that location, the droplet velocity is ~4 m/s (indicated by the vertical line). However, in the case shown in Fig. 4(b), the droplet reaches its stable condition within 0.12 m beyond the injection location, where the droplet velocity is ~20 m/s (indicated by the vertical line). Mesh sensitivity studies are performed on 0.54 and 1.98 million meshes. Results show that the error range is within 0.44% and shows reasonable prediction capability.

Comparisons between the two cases are summarized in Table 4, in which the droplet diameter calculation based on the conventional initial Weber number is clearly under-estimated compared to the Eulerian-Lagrangian method proposed in this study. Especially in the high gas velocity case, the difference between the D_{max} predicted using the initial Weber number and the proposed method is almost two-fold.

To confirm the validity of the proposed approach, three methods for predicting D_{max}, the initial Weber number, the Pilch model [11], and the approach proposed in this study, were compared against four referenced experimental data sets with the results shown in Fig. 5.

Table 4
Comparison of predicted D_{max} results.

Vg (m/s)	D_{max} (micron)	
	Initial Weber number	This study
30 m/s	819	970
75 m/s	131	260

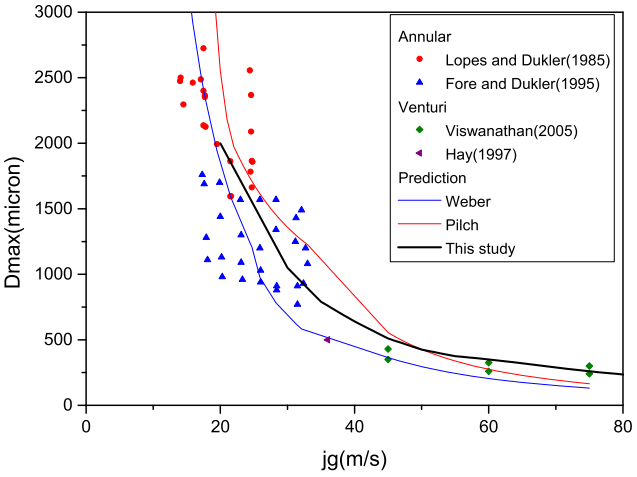

Fig. 5. Comparison of different calculations of maximum droplet size.

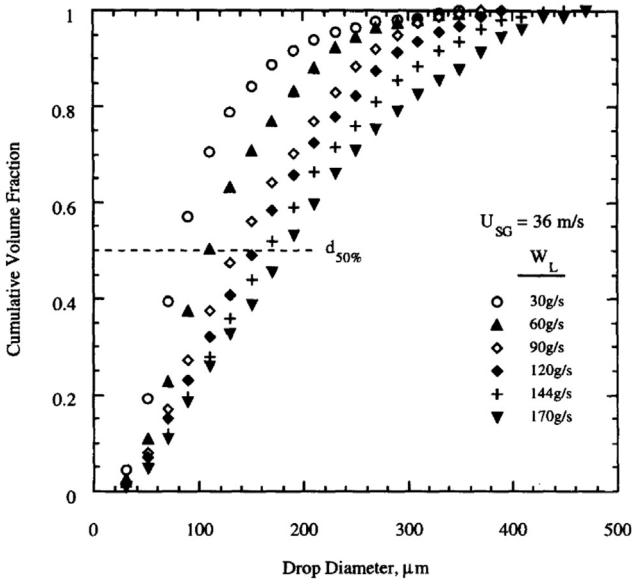

Fig. 6. Effect of L/G on droplet size distribution [21].

The experimental data itself exhibits some scattering mainly due to the different hydraulic conditions, measurement techniques, and experimental setups of each referenced data set. In general, the method proposed in this study shows a reasonable predictive capability over the considered range compared to the other models. In particular, this study predicts the D_{max} relatively well in the high-gas velocity region, while the other models significantly underestimate the D_{max}. This indicates that in order to obtain a better estimate of D_{max} during breakup under high Weber numbers, multistage breakup and droplet acceleration need to be carefully considered.

To determine the ULLN distribution, three parameters, D_{max}, a, and δ, need to be determined. For D_{max}, the CFD calculation results

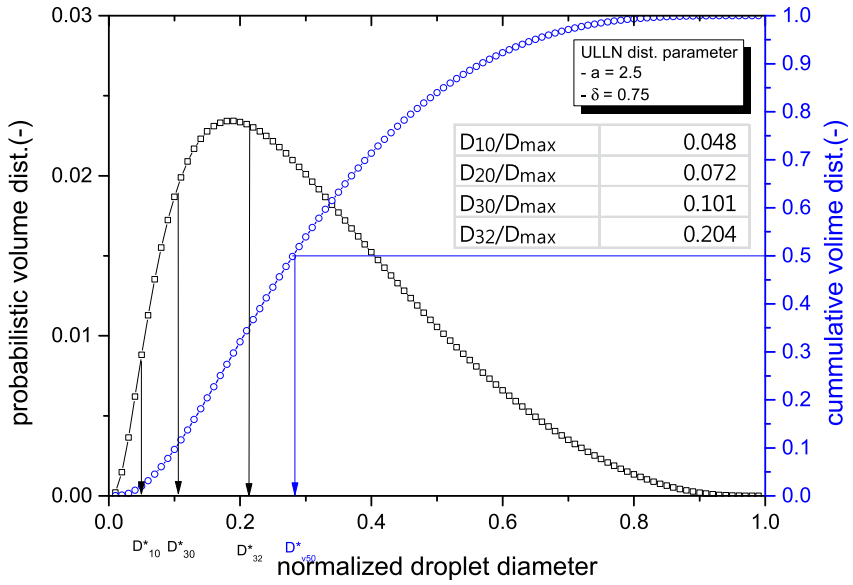

Fig. 7. Proposed normalized ULLN distribution.

Table 5
Venturi scrubber experimental D_{32} data.

Study	Gas velocity (m/s)	L/G (liter/m^3)	Throat size (m)	Throat length (m)
Boll et al. (1974) [8]	30–90	0.6–2.5	0.35x0.305	0.305
Atkinson and Strauss (1978) [30]	50	0.2	0.016x0.04	0.026
Alonso et al. (2001) [15]	70–90	0.5–1.0	0.019 diameter	0.064
Costa et al. (2004) [31]	60–75	0.1–0.3	0.035x0.024	0.14
Viswanathan et al. (2005) [32]	45–75	0.4–1.8	0.152x0.076	0.267
Guerra et al. (2009) [33]	60–75	0.07–0.3	0.04x0.027	0.24

were used. The value of δ, as described in Fig. 2 and Table 1, was determined based on existing experimental data, but was not significantly sensitive to droplet size distribution. As a result, a generally acceptable value of 0.75 was used. For the value of a, the best fit of the experimental results of D_{32} was applied. It is important to note that many results show that as L/G increases, the droplet size distribution becomes more uniform. That means the volume median droplet size (Dv50) increased mainly due to coalescence because of higher probability of collision as L/G increases. A typical trend was shown by Hay et al. [21] and can be seen in Fig. 6.

To reflect this experimental results, correlation factor that best fit the ULLN distribution parameter of a, that representing the ratio of Dv50/D_{max}, is suggested as shown in Eq. (15).:

$$a = \frac{d_{max}}{d_{v50}} - 1 = a_0/(1+f) \tag{15}$$

where $a_0 = 2.5$ and $f = 0.6(L/G - 1)$ if L/G > 1.0.

The final proposed ULLN distribution and its relationship to several other representative droplet diameters is shown in Fig. 7.

3.3. Comparisons of the proposed ULLN CFD model with Boll and Nukiyama Tanasawa model

The proposed methodology for determining the droplet size in a venturi scrubber was validated by existing experimental data for the venturi scrubber. Table 5 summarizes the published experimental data available for D_{32} in the venturi scrubber.

Among the experiments listed in Table 5, Costa et al. [31] and Guerra et al. [33] performed experiments using a relatively small L/G range. Their experimental results showed a large scattering of D_{32} against the value of L/G. In some data, the droplet size decreased as L/G increased, against the general trend. Guerra [33] pointed out that their values for L/G were smaller than those of other studies, thus the results from these studies could not be directly compared. Therefore, in the comparison in this study, the data from Costa et al. [31] and Guerra et al. [33] for values of L/G < 0.15 were excluded.

Comparisons of the resulting D_{32} were then performed between the Boll model, the NT model, and the proposed model, shown in Fig. 8 and summarized in Table 6.

The deviation index and tendency index, defined by Gonçalves [5], and the normalized root mean square difference (RMSD) were then analyzed as follows, with the results as shown in Table 6

$$\text{Deviation Index} \equiv \frac{\sum_{i=1}^{n}\left(abs\left(D_{32,\,predicted} - D_{32,\,measured}\right)/D_{32,measured}\right)_i}{n} \tag{16}$$

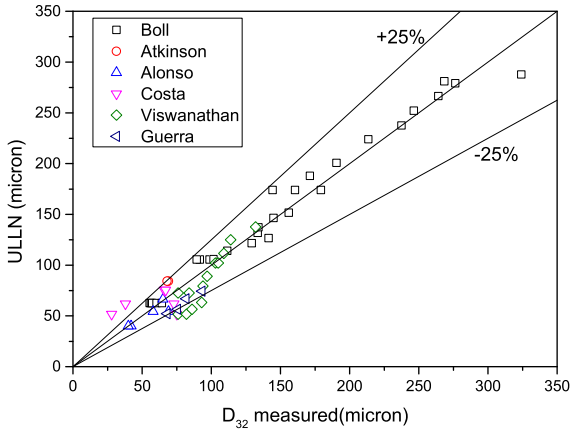

(a) Boll model

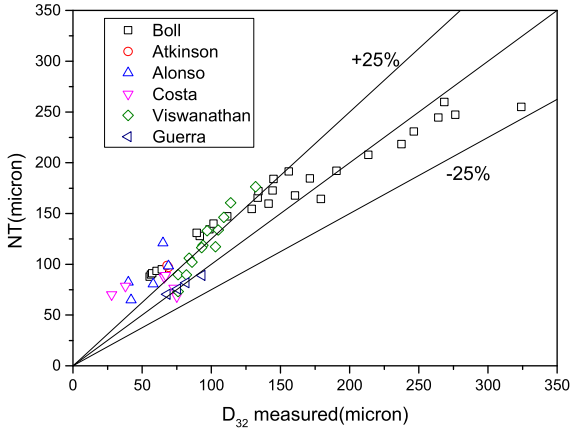

(b) NT model

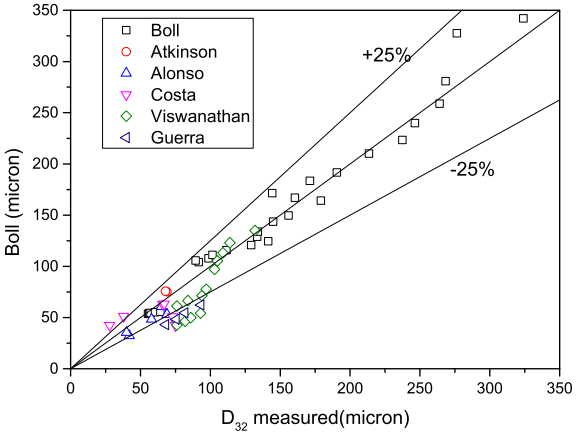

(c) Proposed model

Fig. 8. Comparison between D_{32} calculation results.

Table 6
D_{32} error analysis results.

Model	Deviation (%)	Tendency (%)	NRMSD (%)	Pearson
Boll	16	−7	15.5	0.976
NT	31	27	27.9	0.938
Current study	13	0.4	15.2	0.970

$$\text{Tendency Index} \equiv \frac{\sum_{i=1}^{n}\left(\frac{D_{32,\ predicted}-D_{32,\ measured}}{D_{32,measured}}\right)_i}{n} \tag{17}$$

where a positive value indicates overestimation and a negative value indicates underestimation;

$$\text{Normalized RMSD} \equiv \frac{\sqrt{\sum_{i=1}^{n}\left(\frac{D_{32,\ predicted}-D_{32,\ measured}}{n}\right)_i^2}}{\overline{D}_{32,measured}} \tag{18}$$

The results of the comparison on deviation index show that the proposed model provides superior predictions when compared to the other models. As for tendency index, the Boll model slightly underestimated and the NT model significantly overestimated the overall trend. However, the proposed model exhibited no directional bias.

4. Droplet size prediction model for 1-D calculations

In this section, for more practical purpose minimizing computational complexity, we developed the simple, one dimensional (1-D) calculation of D_{32}. And we compared its predictions with the previously discussed CFD results for an unknown variable of droplet velocity and maximum droplet diameter. In actual conditions, when a droplet interacts with a gas stream, the gas velocity decreases locally due to the transfer of its momentum to the droplet. For the 1-D calculation, the gas velocity is assumed to be constant and equal to the inlet velocity. The governing equations for the 1-D calculation are summarized in Table 7.

Fig. 9 shows the calculation results and comparison between the previously discussed CFD results and those of the 1D calculation. The droplet velocity determined by the CFD calculation exhibits some scattering because the droplet radial distribution is not uniform. However, the overall droplet size can be observed to be reasonably predicted.

Fig. 10 shows the values of D_{max} calculated using three different calculation methodologies. The initial Weber number calculation results are underestimated while the CFD and 1D calculation results are within an acceptable error range. Therefore, the 1D calculation using the governing equation sets listed in Table 7 are applicable when estimating D_{max}.

5. Conclusions

A model for the prediction of the maximum stable droplet diameter during breakup in a venturi scrubber is proposed. The proposed model simultaneously solves the Lagrangian particle tracking of a droplet and the Reitz-Diwakar breakup model using the ANSYS CFX 16 software package. Compared to the proposed model, the conventional model based on the critical Weber number and an instantaneous breakup assumption was observed to significantly under-estimate the maximum droplet size. The proposed model accurately reflected the effects of multi-stage breakup

Table 7
Summary of governing equations for the 1-D calculations.

Unknown variables	Governing equation		Remark
$v_d(z)$	Force balance	$F_D = \frac{d}{dt}\left(\frac{\pi D_d^3}{6}\rho_d v_d\right) = C_D\left(\frac{\pi D_d^2}{4}\right)\frac{\rho_g(v_g - v_d)^2}{2}$	Constant *Vg*
	Drag coefficient	$C_D = \frac{24}{Re_d}(1 + 0.15Re_d^{0.687})$	Shiller-Naumann
$D_d(z)$	Breakup model	$\frac{dD_d}{dt} = -\frac{D_d - D_{d,stable}}{t_b}$	Reitz-Diwakar
	Weber number	$D_{d,stable} = We_{crit}\frac{\sigma}{\rho_g(V_g - V_d)^2}$	$We_{crit} = 12$
$D_{32}(z)$	ULLN distribution	$\frac{D_{32}}{D_d} = \frac{1}{\left(1 + ae^{1/4\delta^2}\right)}$	

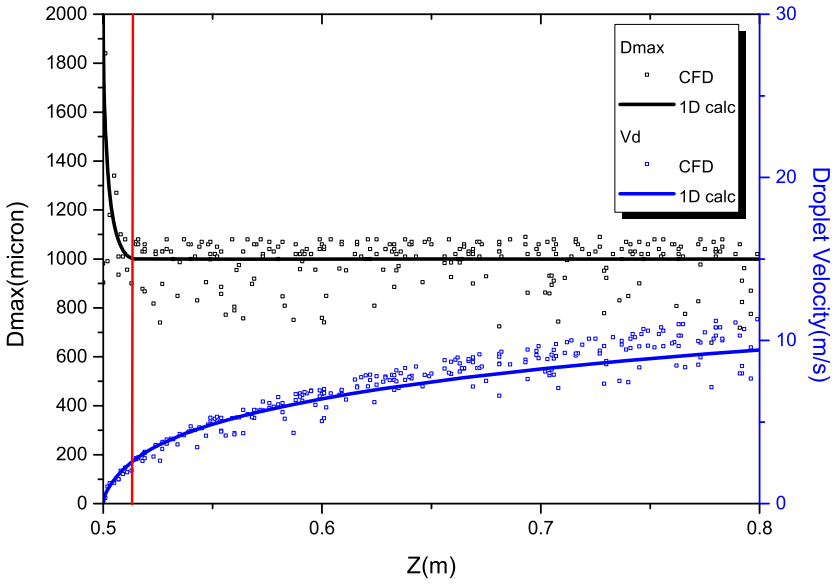

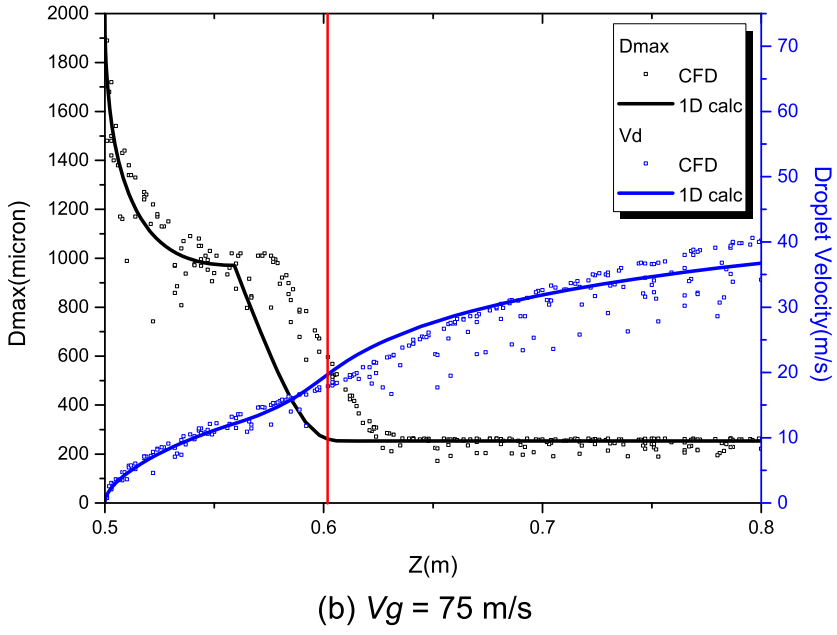

Fig. 9. Comparison of the results of CFD and 1D calculations.

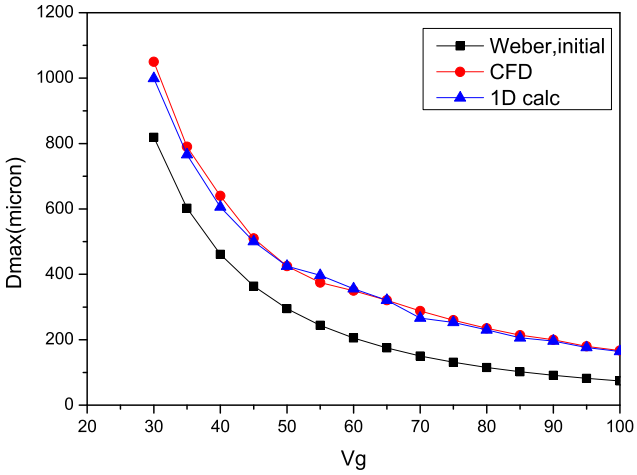

Fig. 10. Comparison of D_{max} prediction for different gas velocities *Vg*.

and droplet acceleration during breakup. Results demonstrate that the proposed model for stable droplet diameter provides better predictions using existing experimental data, especially under a high Weber number.

As a well-known droplet size distribution function, the ULLN distribution function requires three distribution parameters: D_{max}, a, and δ. For D_{max}, the calculation results using the proposed method were used, while the values of a and δ were selected using values that best fit the existing experimental data. Furthermore, the effects of L/G were considered. The comparison of results against experimental data for D_{32} in venturi scrubber geometry indicated that the proposed model provides better predictions than existing empirical correlations, such as those proposed by Boll et al. [8] and Nukiyama and Tanasawa [7].

In this works, effect of liquid film on droplet size is not considered. So, in future work, the effect of liquid film fraction and the entrainment-induced droplet size need to be further examined for technical completeness.

Conflicts of interest

All authors have no conflicts of interest to declare.

Acknowledgement

This research is supported by Korea Hydro & Nuclear Power Co., under the R&D program supervised by KHNP Central research institute.

Nomenclature

A_d	cross-sectional area of droplet [m^2]
a	Upper Limit Log Normal distribution parameter [−]
C_d	drag coefficient [-]
$\overline{d}$	Rosin Rammler distribution parameter that droplet diameter that 63.2% of the total mass is in smaller diameter [m]
D_0	Initial droplet diameter [m]
D_{10}	Arithmetic mean diameter [m]
D_{30}	Volume mean diameter [m]
D_{32}	Sauter mean diameter [m]
D_d	Droplet diameter during breakup [m]
$D_{d,stable}$	Stable droplet diameter assuming instantaneous breakup [m]
D_{max}	Maximum stable droplet diameter [m]
d_{v10}	droplet diameter for 10th percentiles of total droplet volume [m]
d_{v50}	droplet diameter for 50th percentiles of total droplet volume, volume median diameter [m]
d_{v90}	droplet diameter for 90th percentiles of total droplet volume [m]
L/G	Liquid to gas ratio [liter/m^3]
m_d	Single droplet mass [kg]
$\dot{m}_d$	Droplet mass flowrate [kg/s]
$\dot{n}_d$	droplet number rate [#/s]
NT	Nukiyama and Tanasawa
q	Rosin Rammler distribution parameter
Re_d	Droplet Reynolds number
RR	Rosin Rammler
S	Momentum source term [Ns]
ULLN	Upper Limit Log Normal
U	Velocity [m/s]
U_r	Relative velocity [m/s]
F_3	cumulative volume distribution function [−]
f_3	probabilistic volume distribution function [−]
x	traveling distance of droplet [m]

Greek letters

μ	viscosity [$N\,s/m^2$]
ρ	density [kg/m^3]
σ	surface tension [N/m]
δ	ULLN distribution parameter [−]
τ_b	Lifetime of unstable droplet [s]
Γ	Gamma function [−]

Subscript

d	droplet
l	liquid
g	gas
0	initial

References

[1] V.G. Guerra, J.A.S. Gonçalves, J.R. Coury, Experimental verification of the effect of liquid deposition on droplet size measured in a rectangular venturi scrubber, Chem. Eng. Process: Process Intensification 50 (11–12) (2011) 1137–1142.
[2] M. Ali, C.Q. Yan, Z.N. Sun, H. Gu, K. Mehboob, Iodine removal efficiency in non-submerged and submerged self-priming venturi scrubber, Nucl. Eng. Technol. 45 (2013) 203–210.
[3] M. Lehner, Aerosol separation efficiency of a venturi scrubber working in self-priming mode, Aerosol Sci. Technol. 28 (5) (1998) 389–402.
[4] J.C. Lee, W.H. Jung, H.C. Lee, G.T. Kim, D.Y. Lee, Experimental study on aerosol scrubbing efficiency of self-priming venturi scrubber submerged in water pool, Ann. Nucl. Energy 114 (2018) 571–585.
[5] J.A.S. Gonçalves, et al., Evaluation of the models available for the prediction of pressure drop in venturi scrubbers, J. Hazard Mater. 81 (1–2) (2001) 123–140.
[6] C. Berna, et al., Review of droplet entrainment in annular flow: characterization of the entrained droplets, Prog. Nucl. Energy 79 (2015) 64–86.
[7] S. Nukiyama, Y. Tanasawa, An experiment on the atomization of liquid by means of an air stream (1. Report), Trans. Jap. Soc. Mech. Eng. Ser. A 4 (14) (1938) 128–135.
[8] R. Boll, et al., Mean drop size in a full scale venturi scrubber via transmissometer, J. Air Pollut. Control Assoc. 24 (10) (1974) 934–938.
[9] B. Azzopardi, Drop sizes in annular two-phase flow, Exp. Fluid 3 (1) (1985) 53–59.
[10] L.-P. Hsiang, G. Faeth, Drop deformation and breakup due to shock wave and steady disturbances, Int. J. Multiph. Flow 21 (4) (1995) 545–560.
[11] M. Pilch, C. Erdman, Use of breakup time data and velocity history data to predict the maximum size of stable fragments for acceleration-induced breakup of a liquid drop, Int. J. Multiph. Flow 13 (6) (1987) 741–757.
[12] R. Mugele, H. Evans, Droplet size distribution in sprays, Ind. Eng. Chem. 43 (6) (1951) 1317–1324.
[13] L.P. Bayvel, The effect of the polydispersity of drops on the efficiency of a venturi scrubber, Trans. Inst. Chem. Eng. 60 (1) (1982) 31–34.
[14] B. Azzopardi, Drops in annular two-phase flow, Int. J. Multiph. Flow 23 (1997) 1–53.

[15] D. Fernández Alonso, et al., Drop size measurements in venturi scrubbers, Chem. Eng. Sci. 56 (16) (2001) 4901–4911.
[16] D.F. Tatterson, J.C. Dallman, T.J. Hanratty, Drop sizes in annular gas-liquid flows, AIChE 23 (1) (1977) 68–76.
[17] M. Wicks, A. Dukler, In situ measurements of drop size distribution in 2-phase flow-A new method for electrically conducting liquids, Chem. Eng. Prog. 62 (8) (1966).
[18] L.B. Cousins, G.F. Hewitt, Liquid Phase Mass Transfer in Annular Two-phase Flow, Atomic Energy Research Establishment, Harwell, 1968.
[19] J.C. Lopes, A. Dukler, Droplet Sizes, Dynamics and Deposition in Vertical Annular Flow, Dept. of Chemical Engineering, TX (USA), 1985. Houston Univ.
[20] G. Kocamustafaogullari, S. Smits, J. Razi, Maximum and mean droplet sizes in annular two-phase flow, Int. J. Heat Mass Transf. 37 (6) (1994) 955–965.
[21] K. Hay, Z.-C. Liu, T. Hanratty, Relation of deposition to drop size when the rate law is nonlinear, Int. J. Multiph. Flow 22 (5) (1996) 829–848.
[22] V.G. Guerra, et al., Pressure drop and liquid distribution in a venturi scrubber: experimental data and CFD Simulation, Ind. Eng. Chem. Res. 51 (23) (2012) 8049–8060.
[23] S.I. Pak, K.S. Chang, Performance estimation of a venturi scrubber using a computational model for capturing dust particles with liquid spray, J. Hazard Mater. 138 (3) (2006) 560–573.
[24] CFX 16.1 Solver Theory Guide - Particle Transport I, ANSYS, 2015.
[25] R.D. Reitz, R. Diwakar, Structure of High-Pressure Fuel Sprays, 1987. SAE Technical Paper Series 870598.
[26] R. Schmehl, G. Maier, S. Wittig, CFD analysis of fuel atomization, secondary droplet breakup and spray dispersion in the premix duct of a LPP combustor, in: ICLASS 2000: 8th International Conference on Liquid Atomization and Spray Systems, ILASS, Pasadena, CA, USA, 2000, 16-20 July 2000.
[27] F.X. Tanner, Development and validation of a cascade atomization and drop breakup model for high-velocity dense sprays, Atomization Sprays 14 (3) (2004).
[28] W. Reinecke, G. Waldman, A Study of Drop Breakup behind Strong Shocks with Applications to Flight, AVCO SYSTEMS DIV WILMINGTON MA, 1970.
[29] J. Nicholls, Steam and droplet breakup by shock waves, NASA SP 194 (1972).
[30] D. Atkinson, W. Strauss, Droplet size and surface tension in venturi scrubbers, J. Air Pollut. Control Assoc. 28 (11) (1978) 1114–1118.
[31] M. Costa, et al., Droplet size in a rectangular venturi scrubber, Braz. J. Chem. Eng. 21 (2) (2004) 335–343.
[32] S. Viswanathan, D.S. Lim, M.B. Ray, Measurement of drop size and distribution in an annular two-phase, two-component flow occurring in a venturi scrubber, Ind. Eng. Chem. Res. 44 (19) (2005) 7458–7468.
[33] V.G. Guerra, J.A.S. Gonçalves, J.R. Coury, Experimental investigation on the effect of liquid injection by multiple orifices in the formation of droplets in a Venturi scrubber, J. Hazard Mater. 161 (1) (2009) 351–359.